76

GA-A22787

CONF-971103--

RADIATIVE DIVERTOR PLASMAS WITH CONVECTION IN DIII-D

by
A.W. LEONARD, G.D. PORTER, R.D. WOOD,
S.L. ALLEN, J.A. BOEDO, N.H. BROOKS, T.E. EVANS,
M.E. FENSTERMACHER, D.N. HILL, R.C. ISLER, C.J. LASNIER,
R.D. LEHMER, M.A. MAHDAVI, R. MAINGI, R.A. MOYER,
T.W. PETRIE, M.J. SCHAFFER, M.R. WADE, J.G. WATKINS,
W.P. WEST, and D.G. WHYTE

JANUARY 1998

GENERAL ATOMICS

DISCLAIMER

GA–A22787

RADIATIVE DIVERTOR PLASMAS WITH CONVECTION IN DIII–D

by

A.W. LEONARD, G.D. PORTER,* R.D. WOOD,* S.L. ALLEN,* J.A. BOEDO,† N.H. BROOKS, T.E. EVANS, M.E. FENSTERMACHER,* D.N. HILL,* R.C. ISLER,‡ C.J. LASNIER,* R.D. LEHMER,† M.A. MAHDAVI, R. MAINGI,‡ R.A. MOYER,† T.W. PETRIE, M.J. SCHAFFER, M.R. WADE,‡ J.G. WATKINS,# W.P. WEST, and D.G. WHYTE†

This is a preprint of an invited paper presented at the Thirty-Ninth Annual Meeting of the Division of Plasma Physics, November 17–21, 1997, in Pittsburgh, Pennsylvania and to be published in *Phys. Plasmas.*

*Lawrence Livermore National Laboratory, Livermore, California.

†University of California, San Diego, La Jolla, California.

‡Oak Ridge National Laboratory, Oak Ridge, Tennessee.

#Sandia National Laboratory, Albuquerque, New Mexico.

Work supported by
the U.S. Department of Energy under
Contract Nos. DE-AC03-89ER51114, W-7405-ENG-48,
DE-AC05-96OR22464, DE-AC04-94AL85000,
and Grant No. DE-FG03-95ER54294

GA PROJECT 3466
JANUARY 1998

ABSTRACT

The radiation of divertor heat flux on DIII–D [J. Luxon *et al.,* in *Proceedings of the 11th International Conference on Plasma Physics and Controlled Nuclear Fusion* (International Atomic Energy Agency, Vienna, 1987), p. 159] is shown to greatly exceed the limits imposed by assumptions of energy transport dominated by electron thermal conduction parallel to the magnetic field. Approximately 90% of the power flowing into the divertor is dissipated through low Z radiation and plasma recombination. The dissipation is made possible by an extended region of low electron temperature in the divertor. A one-dimensional analysis of the parallel heat flux finds that the electron temperature profile is incompatible with conduction dominated parallel transport. Plasma flow at up to the ion acoustic speed, produced by upstream ionization, can account for the parallel heat flux. Modeling with the two-dimensional fluid code UEDGE [T. Rognlien, J.L. Milovich, M.E. Rensink, and G.D. Porter, J. Nucl. Mater. **196–198**, 347 (1992)] has reproduced many of the observed experimental features.

I. INTRODUCTION

The study of radiating divertor plasmas in order to control target plate heat flux continues to be an important topic for the magnetic fusion program. The design for the power-plant-sized International Thermonuclear Experimental Reactor[1] (ITER) tokamak requires that ~80% of the 300 MW of alpha-particle heating power be dissipated through radiation before deposition on the divertor plates. A significant fraction of this radiation should come from the divertor region to minimize degradation of the core plasma confinement. It is desirable to produce as much radiation from low Z impurities as possible in order to limit high Z contamination of the core plasma. Low Z impurities, such as carbon and beryllium can radiate very efficiently, but usually only at low electron temperature, $T_e < 15$ eV.

It is also important to reduce the particle flux to the divertor target. Even at low T_e, high particle flux can lead to high heat flux due to the ionization and molecular potential energy that is given up as ions and electrons recombine into molecules in the target. Particle flux can also cause excessive target plate erosion. The particle flux can be reduced if plasma conditions allow for significant plasma recombination above the divertor target. Typically, significant recombination will require dense cold plasmas with $T_e \leq 1$ eV. For these two processes, low Z impurity radiation and plasma recombination, to significantly reduce the heat flux in a high power divertor a significant fraction of the divertor volume must sustain dense cold plasma. Parallel energy transport, however is very dependent upon the plasma electron temperature. Therefore it is very important to study the parallel transport processes that will determine the divertor plasma profiles under high power conditions.

The transport of energy parallel to the magnetic field in the scrape-off-layer (SOL) can be described by,[2]

$$\frac{d}{ds}\left[-\kappa T_e^{5/2}\frac{dT_e}{ds}+nv_{||}\left\{\frac{5}{2}(T_i+T_e)+\frac{1}{2}m_i v_{||}^2+I_o\right\}\right]=S_E \qquad (1)$$

where s is the parallel field line length, κ is the parallel electron thermal conductivity, T_e and T_i are the electron and ion temperatures respectively, n is the plasma density, m_i is the ion mass, $v_{||}$ is the plasma fluid velocity parallel to the magnetic field, I_o is the atomic ionization and molecular potential (13.6 eV + 2.2 eV for a deuterium atom) and S_E represents volume sources and sinks of energy such as radiation, ionization, neutral collisions and charge-exchange, and ohmic heating due to any SOL currents. In this formulation we have included the ionization potential in the plasma energy transport because we do not experimentally determine the ionization distribution, an energy sink, nor do we determine the fraction of radiation and target plate heat flux that results from plasma recombination. Instead we combine the competing ionization and recombination terms into a potential carried by the plasma. Also, we have combined the electron and ion energy and disregarded ion viscosity and perpendicular diffusion of energy. The implications of perpendicular diffusion will be discussed later.

Although most all of the transport processes are typically included in two-dimensional (2D) modeling codes, one-dimensional (1D) analytic models are often used to estimate scaling of radiated power fractions. These analytic models typically assume that parallel energy transport is dominated by thermal electron conduction through the bulk of the SOL and divertor plasma. Convection is then significant only in a narrow layer above the target where recycling neutrals increase the plasma flow and energy is carried by convection across the sheath to the divertor target. Electron conduction is given by the first term in the energy transport equation, Eq. (1), or

$q_{||} = -\kappa T_e^{5/2} dT_e/ds_{||}$. Ion conduction is an order of magnitude smaller for $T_i = T_e$ and has been neglected. We will show conduction is a good assumption for typical DIII–D High-confinement (H–mode) divertor plasmas which operate at higher temperature, $T_e \geq 30$ eV, and low radiative losses. However, for radiative divertors it has often been argued[3,4] that this assumption leads to severe localization of the intense radiating region along the field lines and ultimately limits the fraction of heat flux that can be radiated before the field lines strike the divertor target. This is due to the strong $T_e^{5/2}$ dependence of electron heat conduction which results in very short spatial scales of the T_e gradient at high power densities and low temperatures where deuterium and impurities radiate most effectively. For conductive transport the parallel length with plasma $T_e < T_{max}$, can be obtained by integrating the conduction term, or $\Delta L = \frac{2}{7}\kappa T_{max}^{7/2}/q$. Here T_{max} is the maximum temperature at which low Z impurities will radiate efficiently, typically ~15 eV. As an example, in DIII–D with conduction dominated transport of moderate energy flux densities of $q_{||} \geq 50$ MW/m^2, T_e will rise above 15 eV in less than 0.2 m of parallel length from the strike-point. This results in a very small volume of the divertor with plasma conditions appropriate for intense radiation and ultimately recombination. Radiation from carbon, the dominant impurity in DIII–D, peaks at $T_e \leq 15$ eV and drops by more than an order of magnitude[5] by $T_e \geq 20$ eV. Because of the inverse relationship between scale length and parallel power density, $q_{||}$, this problem becomes much worse for the expected higher power densities expected in future divertors. Non-coronal effects due to charge-exchange or fast ion transport may allow more Low Z radiation at higher T_e, but this effect is expected to be limited.[6] Higher Z impurities, such as argon or krypton may radiate efficiently at higher temperatures, but there are significant limitations to the level of high Z material contamination allowed in the main plasma.

On DIII–D, we have greatly exceeded these constraints of conduction dominated transport. We have produced a strongly radiating divertor with $T_e \leq 10$ eV through most of the divertor. From power balance measurements coupled with divertor plasma density and temperature measurements, we infer that plasma flow, or convection, as represented by the second group of terms in Eq. (1), dominates parallel transport of energy for $T_e \leq 15$ eV in DIII–D plasmas. We will see that the low T_e in the divertor allows the recycling neutrals to travel further upstream before ionization. The region of convective transport is then enlarged from a narrow layer above the target to encompass most of the divertor plasma. Convection provides transport of energy at lower gradients of T_e creating a greater volume of plasma for efficient low Z impurity radiation. Ultimately, a large volume of divertor plasma with very low T_e leads to significant plasma recombination. We reduce the peak heat flux to the divertor plate by greater than a factor of 5 while distributing radiation throughout the divertor. In Fig. 1, the radiation distribution for a radiating divertor in DIII–D is plotted. The variation in radiation intensity from the X–point to the divertor is less than approximately a factor of 2, within a spatial resolution given by the view chords of the bolometer which are also shown in the figure. This profile does not exhibit the highly localized radiation suggested by conductive energy transport. We will show that electron thermal conduction cannot account for the measured distribution of divertor radiation and parallel heat flux. However, plasma convection at the ion sound speed through much of the divertor is consistent with our observations. We will also show that convection allows a sufficient volume of divertor plasma with appropriate conditions for plasma recombination to reduce the target plate heat flux even further.

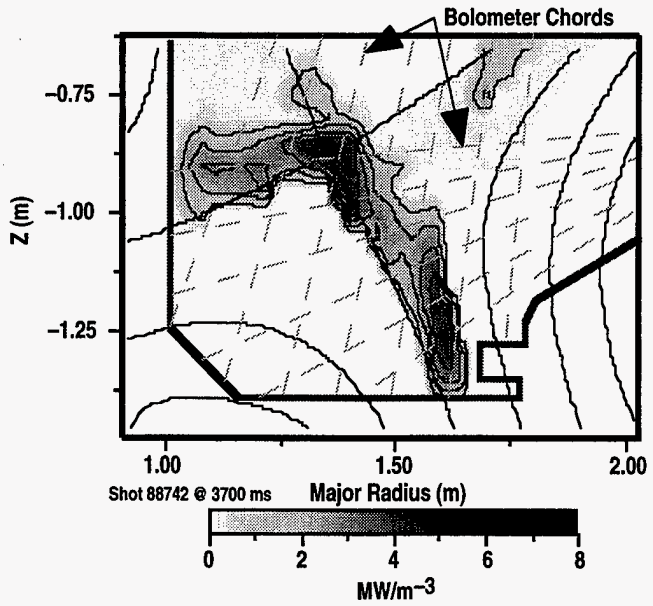

Fig. 1. The radiation profile for radiative divertor operation in DIII–D in an extended geometry configuration. The variation in radiation from X–point to the divertor target is no more than a factor of two within the spatial resolution of the bolometer array whose chords are also shown.

II. PARALLEL ENERGY TRANSPORT

Radiative divertor operation on DIII–D is obtained through additional deuterium gas puffing. A thorough discussion of this mode of divertor operation for DIII-D is given in Ref. 7. For this paper we study H–mode plasmas with a plasma current of 1.4 MA, a safety factor q_{95} of ~4.2 and an injected power of about 4 MW. After H-mode is established deuterium gas is puffed at the rate of ~100 Torr-l/s to establish detached divertor operation. Here "detached" refers to loss of pressure balance between the mid-plane scrape-off layer (SOL) plasma and the divertor target plate. Gas puffing is then reduced to ~25 Torr-l/s in order to maintain the divertor conditions. Typically the peak heat flux to the divertor target is reduced by a factor of 3–5 with a corresponding increase in radiated power. The initial divertor geometry along with the bolometer chord views and divertor Thomson measurement locations are shown in Fig. 2. This X–point location provides three bolometer chords from the horizontal array from the X–point to the divertor for adequate spatial resolution of the radiated power for this analysis. To compare our radiating divertor plasmas to the energy transport described in Eq. (1), divertor sweeping allows divertor Thomson scattering diagnostic[8,9] measurement of the divertor plasma electron temperature and density along flux surfaces.

The power flowing through the outboard divertor leg is described by $\nabla \bullet q_{||} = S_E$ where $q_{||}$ is the parallel heat flux, the sum of conduction and convection, and S_E, the plasma volume sources and sinks of energy, is due principally to atomic radiation. The effects of neutral interactions will be discussed after presentation of the data. Ohmic heating in the SOL, a possible source of energy, is ignored as SOL currents[10] of <50 kA/m^2 are measured for these plasmas and the associated heating represents

a small perturbation to overall power balance. For this analysis we treat the SOL below the X–point as a 1D plasma as a function of $L_{||}$, the field line parallel distance to the divertor plate. The implications of 2D effects such as perpendicular diffusion will be discussed later. The plasma radiation, $\varepsilon\,(L_{||})$, is measured by two poloidally separated 24-channel bolometer arrays whose view chords are shown in Fig. 2. The signals from these two arrays are inverted to produce a 2D radiation profile,[11] as also shown in Fig. 2. This profile is integrated radially through the divertor SOL and with the assumption of toroidal symmetry produces a 1D profile of radiation, $\varepsilon_{sol}(z)$, as a function of distance from the divertor plate. We calculate the total power, $Q_{tot}(z)$, flowing in this 1D divertor approximation by starting with the divertor target heat flux measured by an IR camera[12] and integrating the 1D radiation profile. Contributions from plasma radiation and Edge-Localized Modes (ELMs) are subtracted from the target heat flux. We finally convert to parallel heat flux, $q_{||}\,(L_{||})$, by dividing by the cross-sectional area of the SOL perpendicular to the magnetic field. The SOL area normal to the magnetic field lines is determined by the heat flux width at the divertor plate in conjunction with magnetic equilibrium measurements and remains constant through the divertor assuming constant SOL magnetic flux. The target plate heat flux at the target is only indicative of the width throughout the divertor and SOL. The upstream energy flux width may vary from that at the target due to processes such as perpendicular diffusion or radiative loss fractions that vary on different magnetic flux surfaces. The parallel path length, $L_{||}$ is converted from z by magnetic mapping of a field line in the center of the SOL.

We have subtracted the ELM contributions from the target plate heat flux for this analysis. ELMs are short bursts of energy and particles that are released into the SOL by an instability just inside the separatrix of the main plasma.[13,14] They may temporarily heat the SOL and divertor plasma allowing more power to be conducted for a short time. We are interested in analysis of the steady-state or quiescent

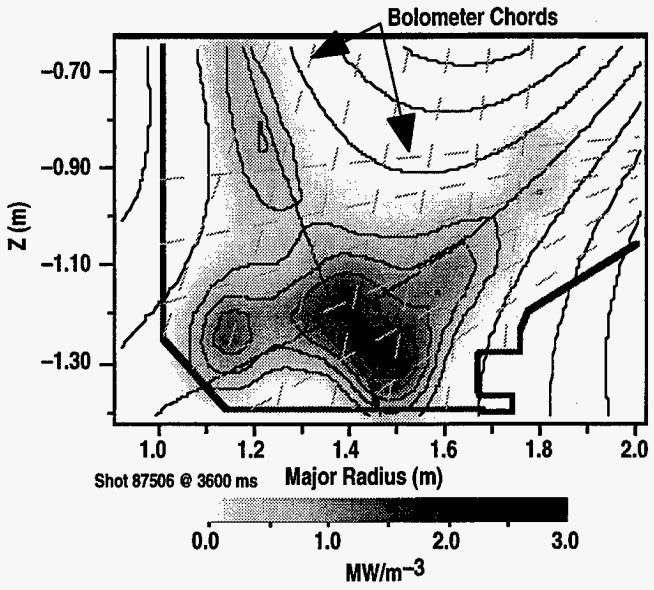

Fig. 2. The geometry and radiation profile for the discharges used in the energy transport analysis. Also shown are the bolometer chords and Thomson scattering diagnostic view locations.

transport of energy. Previous analysis of ELMs on DIII–D[15] has shown that ~20% of the injected power crosses the separatrix during the brief ELM pulse. The resulting ELM pulse on the outboard divertor target represents ~10% of the time-averaged heat flux. This is a small part of the outboard heat flux during standard attached operation, but it becomes a significant fraction of the remaining target plate heat flux during detached radiative operation. This is illustrated by the components of the heat flux profile during radiative divertor operation, plotted in Fig. 3. Approximately one-half of the measured heat flux is due to increased radiation and subsequent heating of the target. Much of the remaining heat flux is due to the ELM pulse. The ELM heat flux remains similar both before and during detached operation. The heat flux from the ELM is typically deposited on the target within 1 ms of the onset of the midplane instability. This is much shorter than the ELM period of ~20 ms. The ELM heat flux represents a real concern for future large tokamak divertors though we do not address that subject in this paper. The low level

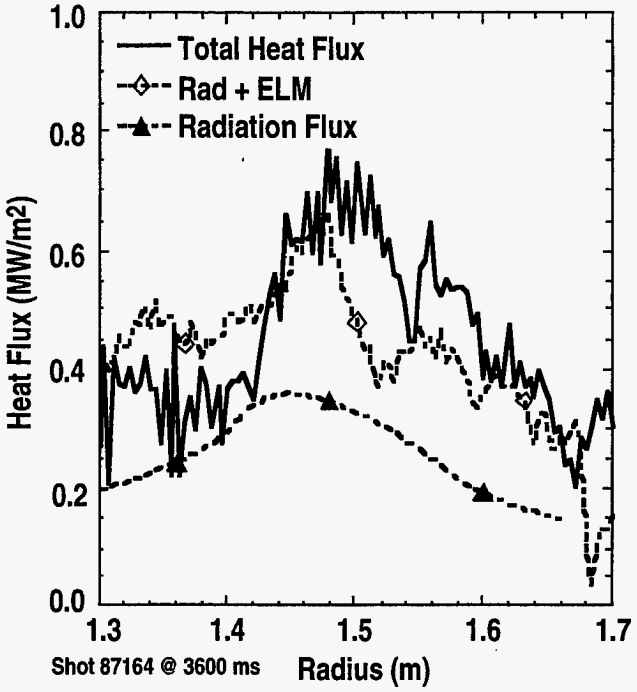

Fig. 3. The target plate heat flux profile in radiative divertor discharges. Also shown are contributions to that heat flux from radiative heating and ELMs.

of heat flux remaining after subtracting the radiation and ELM contributions is consistent with the saturation current measured by divertor target mounted Langmuir probes. It is this remaining heat flux that we use in our energy transport analysis.

We use the techniques described above to first examine attached ELMing H-mode plasmas on DIII-D without large radiative losses in the divertor. We plot in Fig. 4(a) the parallel heat flux, $q_{||}$, vs. the parallel distance from the divertor target, $L_{||}$. Approximately 50 MW/m^2 is flowing into the outboard divertor leg just below the X–point. Only a small fraction of this power, ≤20%, is radiated away and most of it strikes the divertor as target plate heat flux. If parallel electron thermal conduction dominates this measured energy transport we then can calculate the required electron temperature profile by integrating the conductive term of Eq. (1), $q_{||} = -\kappa T_e^{5/2} dT_e/ds$, where $\kappa = 1.55 \times 10^3$ in eV and MKS units for these plasmas. Integrating from the divertor target an electron temperature of 20 eV near the target

we arrive at the conduction fitted T_e profile as plotted in Fig. 4(b). The 20 eV target temperature is measured with divertor plate Langmuir probes and divertor Thomson and is also consistent with a sheath boundary condition with our measured density and target heat flux. We next compare this fitted T_e profile to the profile measured by the divertor Thomson system. The T_e profile is obtained by sweeping the divertor across the Thomson channels and averaging over the same flux space as the target plate heat flux used for the energy flux analysis. The experimentally measured T_e profile, also plotted in Fig. 4(b), increases from ~20 eV near the target to more than 40 eV at the X–point and is consistent with the conduction fitted profile. The density profile, for reference, varies from ~0.5×10^{20} m^{-3} at the divertor target to ~0.3×10^{20} m^{-3} near the X–point.

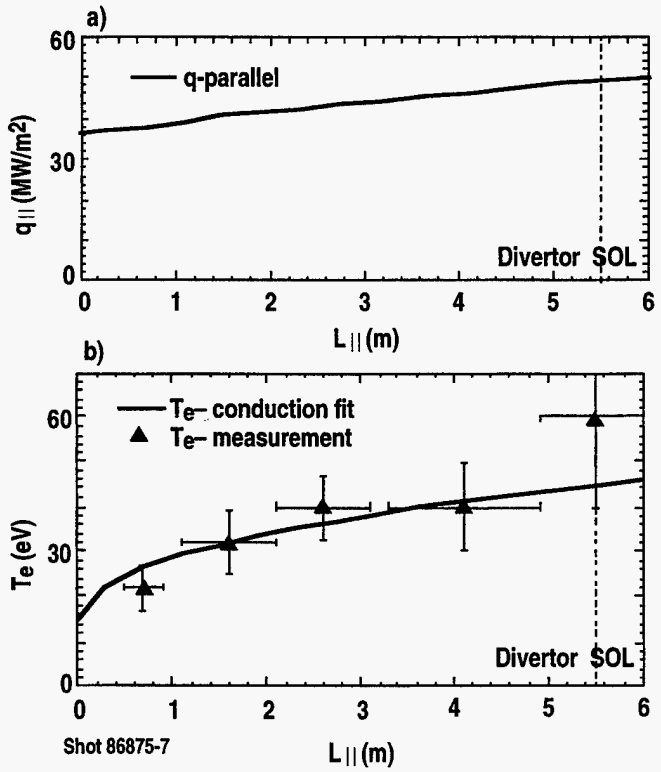

Fig. 4. (a) The parallel heat flux profile in an attached divertor plasma vs. parallel distance from the divertor target. (b) The electron temperature profile required to support the measured heat flux by conduction. Also plotted is the measured electron temperature profile.

For detached operation the divertor becomes radiative with significant heat flux reduction as shown earlier in Figs. 2 and 3. Now, ~20 MW/m^2 of parallel heat flux flows into the divertor X–point region. Most of that heat flux is radiated away leaving ~2 MW/m^2 to strike the divertor target as shown by the heat flux profile in Fig 5(a). The heat flux flowing into the outboard divertor at the X–point is reduced during detached operation for two reasons. First, gas puffing, used to obtain detachment, raises the central and SOL densities resulting in greater upstream radiation and reduced energy flux into the divertor. The rise in SOL and main plasma density is due, at least in part, to the open geometry of the DIII–D divertor where the mid-plane neutral pressure rises significantly with gas puffing. Secondly, the heat flux profile at the divertor target is broader. In this 1D analysis we have taken the target plate heat flux profile as the characteristic width for energy transport. Though the target plate heat flux is very low, it's width is about 50% greater for detached operation. As stated earlier the increased width may result from 2D aspects of energy loss such as increased perpendicular diffusion or varying fractions of radiative losses on different magnetic surfaces. Using the target plate width gives us the correct parallel heat flux at the target, though we may somewhat underestimate the parallel heat flux near the X–point. The uncertainty in the upstream width we estimate at 20%-30%.

During detached operation we have seen a significant decrease in the parallel heat flux profile, particularly near the target. However, as plotted in Fig. 5(b), if conduction is still to dominate parallel energy transport then the electron temperature must still rise above 15 eV in a relatively short parallel distance of $\leq$1 m, or $\leq$5 cm of poloidal length, which is <15% of the total divertor length. This is once again due to the strong $T_e^{5/2}$ dependence for conduction. The experimental profile of electron temperature is also plotted in Fig. 5(b) and is in stark contrast to that expected from conduction dominated transport. The electron density and

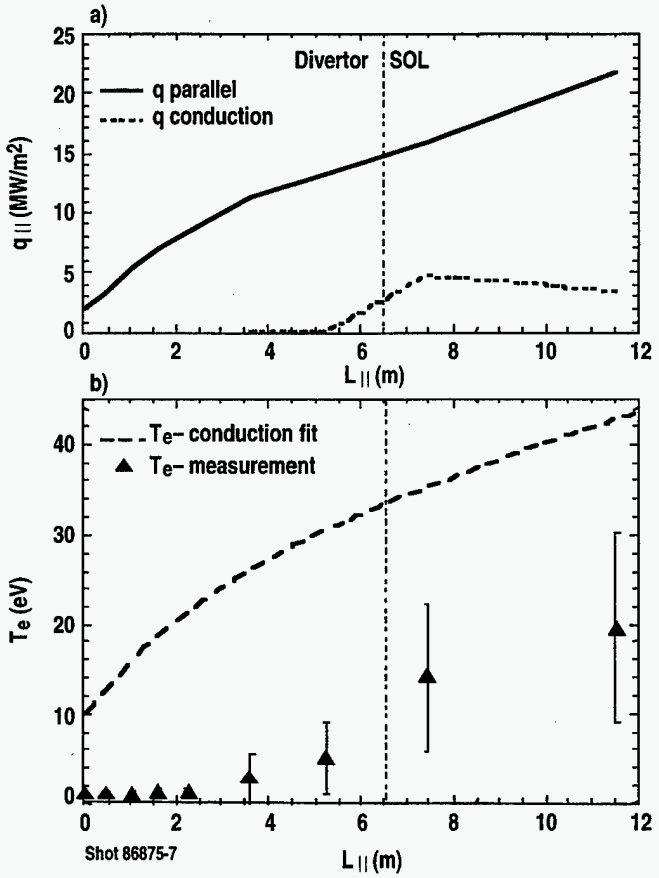

Fig. 5. (a) The parallel heat flux profile in detached, or radiative divertor plasmas. (b) The electron temperature profile required to support the measured heat flux by conduction. Also plotted is the measured electron temperature profile.

pressure profiles are also shown in Fig. 6. For detached operation we see that the T_e profile is now very low, ~1–2 eV throughout the divertor and approaching 5 eV just below the X–point. The electron temperature finally reaches 20 eV above the X–point. Using the electron conduction equation, $q_{||} = -\kappa T_e^{5/2} dT_e/ds$, we plot in Fig. 5(b) the energy flux that our measured T_e profile would support. Through most of the divertor, with $T_e \leq 5$ eV, the temperature gradient can support essentially none of the measured heat flux through conduction. Near the X–point and above this fraction rises to about one-quarter.

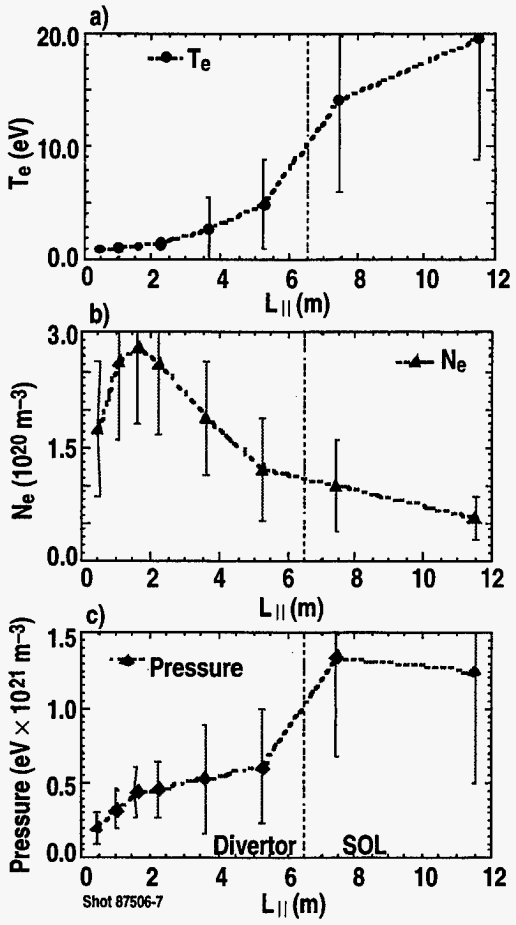

Fig. 6. The divertor plasma parameters during detached operation. Shown are profiles of electron temperature, density and pressure vs. parallel distance from the target.

A non-Maxwellian electron energy distribution might lead to enhanced thermal conduction in the SOL.[16] The hotter less dense SOL plasma above the X-point is much less collisional than the divertor plasma. A higher energy collisionless population of electrons might carry a significant fraction of the energy flux from above the X-point. The plasma in the divertor and near the X-point, however, is very collisional and should thermalize hot electrons very quickly. A 150 eV electron, approximately four times the 40 eV thermal T_e of the mid-plane SOL, will have a slowing distance of ~1 m of parallel length for the divertor plasma of n_e = 3.0×10^{20} and T_e = 2 eV. Such an electron should be thermalized within the region

of the X-point before entering the divertor leg. More work is needed to ascertain the magnitude of the effect on energy transport, but it appears unlikely it can explain our data through the bulk of the divertor.

A vertical viewing Vacuum-Ultra-Violet (VUV) spectrometer measures the radiating constituents of these radiative divertor plasmas. It was previously reported[17,18] that about three-quarters of the radiation is due to carbon. Deduced from line-ratio techniques, most of the carbon radiation originates from plasma with T_e ~ 8–12 eV. From the temperature profile it is seen that this region of plasma exists in the SOL and divertor just outside of the X–point. The remaining plasma radiation is due to neutral deuterium and originates from the divertor down to the target plate. A TV camera tangentially viewing the divertor in visible light[19,20] also observes this distribution of carbon and deuterium radiation. The volume of plasma for T_e ~ 8–12 eV is substantially larger than we would expect from conduction dominated transport. The characteristic parallel length increases to ΔL ~ 1–2 m for this critical range of T_e for maximum carbon radiation. The expanded volume, along with coronal radiation for ~3% carbon impurity is roughly consistent with the measured radiation level.

III. PARALLEL PARTICLE TRANSPORT

It is possible to account for the measured energy flux through parallel plasma flow, or convection. If we assume convection carries the power not conducted we can solve for the required particle flux and flow speed. We use the equation $q_{||} - q_{cond} = nv_{||}\left[5/2(T_e + T_i) + 1/2 m_i v_{||}^2 + I_o\right]$ to represent the convected heat flux and solve for the particle flux, $nv_{||}$, and the flow speed in terms of Mach #, $v_{||}/c_s$, where c_s is the ion acoustic speed given by $c_s = \left[Zk(T_e + T_i)/m_i\right]^{1/2}$. The flow is normalized to the acoustic speed because it represents a boundary at which certain fluid phenomenae may be expected to occur. Here q_{cond} as plotted in Fig. 5(a), is determined from the electron temperature profile. We also assume T_i is to equal T_e, which is expected at these divertor parameters. Solving this equation for the inferred particle flux and Mach # profiles, as plotted in Figs. 7(a) and (b), one sees that our measured heat flux profile can be supported by plasma flow just below the ion acoustic speed in the divertor and ~0.4 times the acoustic speed above the X–point.

The particle flux, or flow, profile is a good indication of where ionization, or production of plasma is taking place. First, as shown in Fig. 7, there is a significant upstream plasma flow. A major fraction of this flow is due to ionization of neutrals in the SOL. In the open divertor geometry of DIII–D neutrals may not be confined to the divertor region, but may make their way around the plasma periphery towards the midplane. This is especially true during detached operation when much of the divertor plasma electron temperature is less than 5 eV leading to an ionization path longer than the scale length of the divertor. The rest of the upstream flow is produced by diffusion of plasma across the separatrix from the main plasma. The main plasma particle source that leads to this diffusion is due to central fueling from

neutral beam injection and ionization of neutrals that make their way across the separatrix.

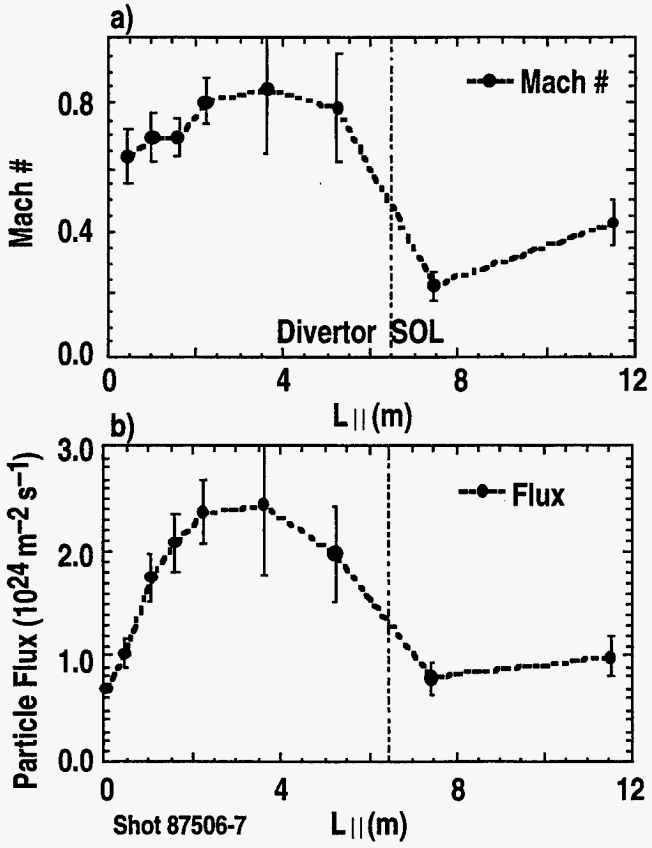

Fig. 7. (a) The parallel particle flux required to support the measured parallel heat flux through conduction. (b) The flow speed of the plasma, in terms of Mach #, implied by the particle flux profile.

In the region of the X–point there is a significant increase in particle flux indicating a region of high ionization. Recycled neutrals from near the target are able to pass through the low temperature region, $T_e \leq 2$ eV, and move up to the vicinity of the X–point. In this region T_e increases from less than 5 eV to ~15 eV resulting in more than an order of magnitude increase in the ionization cross section.[21] Plasma from this ionization region then flows back towards the plate at nearly the ion acoustic speed. This sets up a recirculating flow pattern of neutrals from the target plate to the X–point and plasma from the X–point back to the target.

Finally there is a reduction in the particle flux as the flowing plasma approaches the target plate. Plasma recombination may account for this reduction in flux. The extended region of low temperature, $T_e < 2$ eV, and high density, $n_e > 2 \times 10^{20}$ m^{-3}, may allow significant recombination to take place. The plasma slows somewhat as well, as it flows from the X–point to the divertor target. This can occur from the plasma-neutral interactions. The slowing results in a longer transit time for the flowing plasma allowing a greater fraction of the ions and electrons to recombine. There is still significant uncertainty in determining the fraction of recombined particle flux from our power balance measurements. The error bars in Fig. 7 represent uncertainty in only the average density and temperature. Other factors such as changes in the SOL width would add to the uncertainty. The expected recombination rate due to three-body and radiative processes can be calculated from the measured density and temperature profiles. These rates are less than that inferred from power balance. However, the recombination rate is a strong function of density and temperature and any uncertainty in those measurements will result in large uncertainty in the expected recombination rate. Accurate determination of the recombination rate requires more direct measurements from spectroscopy.

Spectroscopic evidence for recombination has previously been reported in DIII–D detached plasmas[22,23] and other tokamaks as well.[24-27] The absolutely calibrated VUV spectrometer with a vertical view of the divertor simultaneously measures The Lyman-α (L_α) and Lyman-β (L_β) emission from neutral deuterium. A L_α/L_β ratio of about 40 would indicate the emission is generated from a region of ionization. In regions where recombination is the dominant process upper energy levels of neutral deuterium are preferentially populated resulting in a L_α/L_β ratio of about 4. The time evolution of the L_α/L_β ratio during deuterium puffing is shown in Fig. 8. Before gas puffing, with the divertor in the attached condition, the L_α/L_β ratio is about 40 with T_e in the divertor >40 eV. This indicates very little plasma

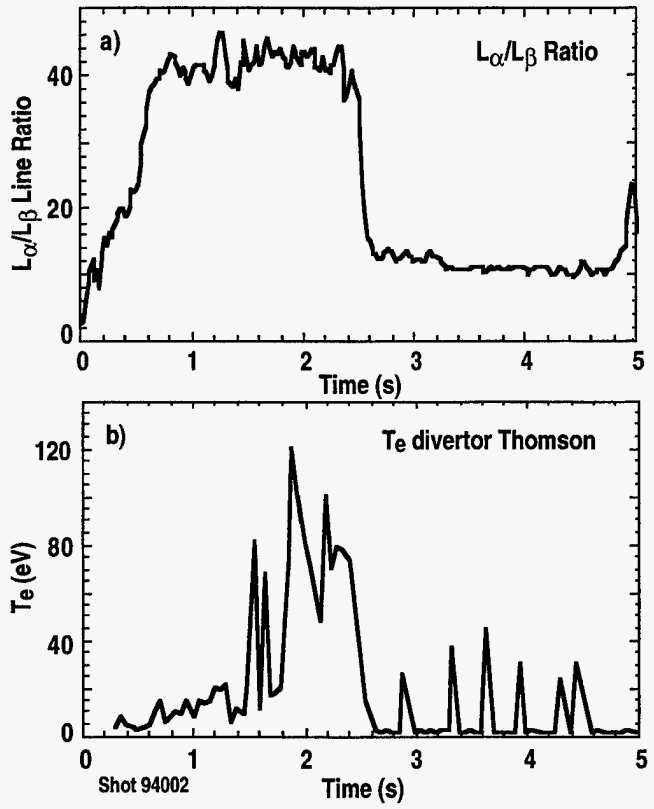

Fig. 8. (a) The ratio of L_α to L_β as measured by a vertical view of the divertor from a VUV spectrometer. The lower ratio after gas puffing indicates plasma recombination is responsible for a significant fraction of the deuterium radiation. (b) The electron temperature of the divertor as measured by Thomson scattering. The higher temperature points after the transition to detached operation are due to ELMs occasionally captured by the diagnostic.

recombination is taking place. Shortly after injecting neutral deuterium a rapid transition to the detached state occurs. The measured T_e in the divertor drops to ~1 eV and the L_α/L_β ratio drops to ~10. The ratio of 10 indicates that approximately half of the observed L_α photons originate from a region where recombination dominates over ionization. More analysis with a consistent data set is required to determine the fraction plasma flux that recombines above the divertor target. The issue of plasma opacity to Lyman radiation must also be addressed in further analysis.[27] These topics will be an area of future DIII–D research.

There are two factors we ignored in our analysis which could have an effect on the parallel heat flux profile and the plasma flow we infer from that. The first is

additional heat loss from neutral interaction with the plasma. Neutrals may carry power out of the plasma through charge-exchange and elastic collisions and would appear as additional heating of the vessel walls. This effect does not appear to be large, however. Much of this neutral heat flux would be deposited on the divertor target where the heat flux is already measured. The IR cameras view the divertor floor inboard and outboard of the strike-point and do not observe significant heat flux from the neutrals. The consequence of any neutral power that is not measured would be a greater parallel heat flux upstream and increased plasma flow to carry the additional power.

Secondly, the 1D analysis above ignores perpendicular transport or other 2D effects. Perpendicular transport can result in the SOL widening from the X–point region to the divertor target. Krasheninnikov[28] has shown that perpendicular transport can lead to a larger volume of plasma at low temperature for more efficient radiation. A wider SOL results in lower heat flux density requiring a smaller temperature gradient for conductive transport. We attempt to take any perpendicular transport into account by taking the heat flux width at the target plate for the SOL heat transport width. Other 2D effects, such as variations in radiated fractions on different surfaces, could also effect our interpretation of the energy flux width. With the heat flux width increasing in the detached state these effects would likely result in a greater upstream heat flux that we have estimated. This would result in greater upstream particle flux with the same conclusion that convection is required to explain the measured heat flux and plasma profiles.

IV. MODELING WITH UEDGE

Simulations with the UEDGE code[29,30] have been run to compare a full 2D description of the plasma to our 1D analysis above. The code contains a two-fluid model of the plasma with classical parallel transport for the ions and electrons and anomalous perpendicular transport for both species. The carbon impurities are generated with physical and chemical sputtering. The carbon ions are modeled with complete impurity transport for all six charge states. The neutrals are described by a Navier-Stokes flux model that permits momentum loss by charge-exchange and ion-neutral collisions.

The UEDGE code has been run to produce stable solutions with detached divertor conditions.[31] In this solution most of the input power is radiated by carbon impurity with little heat flux reaching the target plate. Generation of carbon impurity through chemical sputtering is an important process from obtaining this solution. The plasma electron density and temperature from the UEDGE solution are plotted as a function of parallel distance from the outer target plate in Fig. 9(a). The profiles are averaged over the SOL with a flux width similar to that done in the data analysis. In the UEDGE solution T_e is very low throughout the divertor, $T_e < 2$ eV, with the density reaching a maximum just above the target plate. The recombination zones in the simulation, shown in Fig. 9(b), are also very similar to that inferred from the experimental data. Ionization peaks just below the X–point, leading to plasma flowing towards the target. The plasma cools further as it flows toward the target with the density building until recombination becomes a significant process. The Mach # is also seen to increase just below the X–point in the simulation and then decrease again near the target.

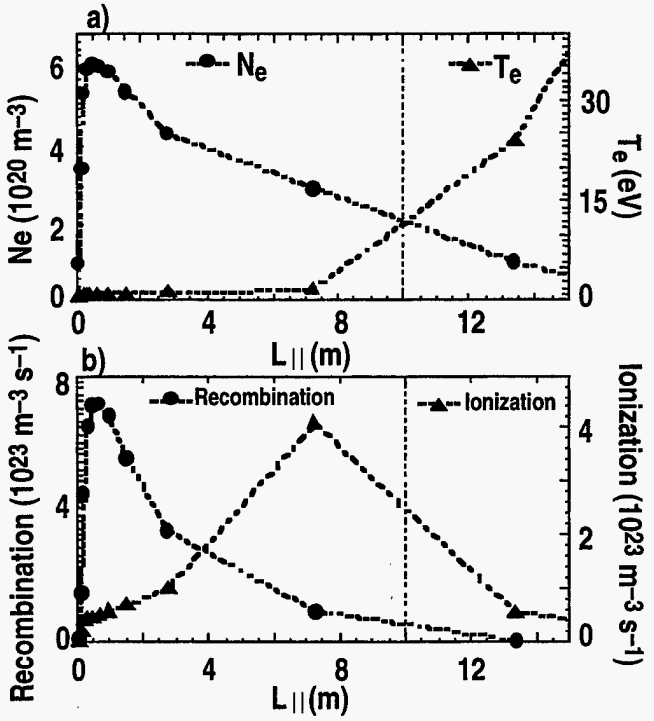

Fig. 9. The (a) electron density and temperature, and (b) the ionization and recombination rates vs. parallel distance from the target plate as simulated by the UEDGE code.

An important aspect the simulation can address is the level of flow achievable in the 10 eV region where carbon is the dominant radiator. In the experiment it appears that core and SOL ionization produce enough flow to expand the volume of plasma at T_e ~ 8–12 eV such that carbon can radiate a large fraction of the input power. For the simulation here the convected and conducted heat fluxes are plotted in Fig. 10. Below the X–point, where T_e is very low, all of the heat flux is due to convection. Above the X–point T_e is about 30 eV and the conducted and convected heat fluxes are about equal. Unfortunately the UEDGE grid is too coarse poloidally to resolve details in the critical 10 eV region. However, even at 30 eV there is enough plasma flow for the convected power to equal the conducted power. By 15 eV the convected fraction could well be dominant. A more accurate simulation with a finer poloidal

resolution coupled to neutral particle modeling with the correct vessel wall may be needed to fully address this issue.

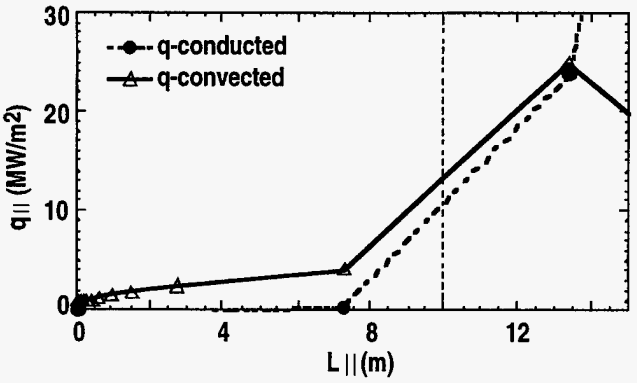

Fig. 10. The conducted and convected parallel heat fluxes versus parallel length from the divertor target as simulated by the UEDGE code.

V. CONCLUSIONS

We have shown that in DIII–D, during radiative divertor conditions, parallel energy transport from the X–point region to the divertor target is dominated by convection. We measure the parallel heat flux profile with power balance techniques and find that electron temperature gradients are too small to support this heat flux through conduction. We then infer the plasma flow profile to supply the remaining heat flux. The plasma flow allows a greater volume of plasma with $T_e \sim 8$–12 eV where carbon can radiate efficiently. Finally the flow allows a large region of plasma with lower temperature, $T_e < 2$ eV, where significant recombination can take place.

The expansion of the low temperature and convection dominated region in the divertor on DIII–D allows for more radiation and recombination than would be estimated by 1D conduction based models of the SOL. In turn, these models may not be very accurate in predicting the levels of low Z radiation and recombination that can be achieved in future higher power divertors. It might be possible, through proper recycling and injection of the working gas to greatly increase the low Z radiation in these future divertors.

Before a future divertor can be designed using these concepts though, much work remains to be done. First, scaling to higher power must be demonstrated. Since the atomic physics of radiation occurs at constant temperature, higher power densities will require greater particle flux, through higher density or flow speed, to sufficiently expand the radiation and recombination regions. The high density or particle flux necessary for future high power divertors may be very difficult to achieve. Characterization and measurement of 2D effects are also necessary for scaling and understanding parallel energy transport. Measurement of the 2D

ionization profile can be used to determine the source of flow in the SOL and divertor. As stated earlier perpendicular transport also can play important role by expanding the SOL width and increasing the radiating volume. Perpendicular transport, perhaps through neutrals or fluctuations, may help produce flow in the higher temperature regions. While most of the ionization to produce flow should take place in the outer SOL where $T_e < 10$ eV, these transport processes may propagate the flow deeper into the SOL at higher temperature.

Finally, a radiating divertor must be made compatible with the high confinement central plasma. The consequences of highly radiating divertor may be a higher midplane separatrix density or increased neutral pressure in the divertor or plasma periphery. These properties may have a significant effect on the main plasma. But also, the requirements of the main plasma for proper performance must be made known. It may be necessary to control the separatrix density or boundary neutral pressure to produce the required main plasma parameters. Knowledge of these boundary conditions will be required to successfully design any future high power divertor.

REFERENCES

[a]Lawrence Livermore National Laboratory, Livermore, California·

[b]Oak Ridge National Laboratory, Oak Ridge, Tennessee.

[c]University of California — San Diego, San Diego, California·

[d]Sandia National Laboratories, Albuquerque, New Mexico.

[1]G. Janeschitz, K. Borass, G. Federici, Y. Igitkhanov, A. Kukushkin, H.D. Pacher, G.W. Pacher, and M. Sugihara , J. Nucl. Mater. **220–222**, 73 (1995).

[2]S.I. Braginskii, "Transport Processes in a Plasma," in "Reviews of Plasma Physics," Vol 1 (M.A. Leontovich, Ed.) Consultants Bureau, New York 1965 p. 205.

[3]K. Lackner, and R. Schneider, Fusion Engineering and Design **22**, 107 (1993).

[4]D. Post, N. Putvinskaya, F.W. Perkins, W. Nevins, J. Nucl Mater. **220-222**, 1015 (1995).

[5]S.L. Allen, M.E. Rensink, D.N. Hill, R.D. Wood, D.G. Nilson, B.G. Logan, R.D. Stambaugh, T.W. Petrie, G.M. Staebler, M.A. Mahdavi, R. Hulse, and R.B. Campbell, J. Nucl. Mater. **196-198**, 804 (1992).

[6]M.A. Mahdavi, G.M. Staebler, R.D. Wood, D.G. Whyte and W.P. West, J. Nucl. Mater. **241-243**, 305 (1997).

[7]T.W. Petrie, D.N. Hill, S.L. Allen, N.H. Brooks, D.A. Buchenauer, J.W. Cuthbertson, T.E. Evans, P. Ghendrih, C.J. Lasnier, A.W. Leonard, R. Maingi, G.D. Porter, D.G. Whyte, R.J. Groebner, R.A. Jong, M.A. Mahdavi, S.J. Thompson, W.P. West, R.D. Wood, Nucl. Fusion **37**, 321 (1997).

[8]T.N. Carlstrom, C.L. Hsieh, R.E. Stockdale, D.G. Nilson, D.N. Hill, Rev. Sci. Instrum. **68**, 1195 (1997).

[9]S.L. Allen, D.N. Hill, T.N. Carlstrom, D.G. Nilson, R.E. Stockdale, C.L. Hsieh, T.W. Petrie, A.W. Leonard, D. Ryutov, G.D. Porter, R. Maingi, M.R. Wade, R. Cohen, W. Nevins, M.E. Fenstermacher, R.D. Wood, C.J. Lasnier, W.P. West, M.D. Brown, J. Nucl. Mater. **241-243**, 595 (1997).

[10]M.J. Schaffer, B.J. Leikind, Nucl. Fusion **31**, 1750 (1991).

[11]A.W. Leonard, W.H. Meyer, B. Geer, D.M. Behne and D.N. Hill, Rev. Sci. Instrum. **66**, 1201 (1995).

[12]D.N. Hill, R. Ellis, W. Ferguson, D.E. Perkins, T.W. Petrie, C.B. Baxi, Rev. Sci. Instrum. **59**, 1878 (1988).

[13]M. Keilhacker, G. Becker, K. Bernhardi, A. Eberhagen, M. El Shaer, G. Fussman, O. Gehre, J. Gernhardt, G. v. Gierke, E. Glock, G. Haas, F. Karger, S. Kissel, O. Kluber, M. Kornherr, K. Lackner, G. Lisitano, G. Lister, J. Massig, H.-M. Mayer, K. McCormick, D. Meisel, E. Meservey, E.R. Muller, H. Murmann, H. Niedermeyer, W. Poschenrieder, H. Rapp, B. Richter, H. Rohr, F. Ryter, F. Schneider, G. Siller, P. Smeulders, F. Soldner, E. Speth, A. Stabler, K. Steinmetz, K.-H. Steuer, Z. Szymanski, G. Venus, O. Vollmer, F. Wagner, Plasma Phys. Controlled Fusion, **26** 49 (1984).

[14]E.J. Doyle, R.J. Groebner, K. H. Burrell, P. Gohil, T,. Lehecka, N.C. Luhmann, Jr., H. Matsumoto, T.H. Osborne, W.A. Peebles, R. Philipona, Phys. Fluids B **3** 2300 (1991).

[15]A.W. Leonard, W. Suttrop, T.H. Osborne, T.E. Evans, D.N. Hill, A. Herrmann, C.J. Lasnier, D.N. Thomas, J.G. Watkins, W.P. West, M. Weinlich, H. Zohm, J. Nucl. Mater. **214-243**, 628 (1997).

[16]O. Batischev, S.I. Kraaheninnikov, R.J. Catto, A.A. Batishcheva, D.J. Sigmar, X.Q. Xu, J.A. Beyers, T.D. Rognlien, R.H. Cohen, M.M. Shoucri, I.P. Shkarofskii, Phys. Plasmas **4**, 1672 (1997).

[17]R.D. Wood, R.C. Isler, S.L. Allen, M.E. Fenstermacher, C.J. Lasnier, A.W. Leonard, and W.P. West, 23rd European Physical Society Conf. on Controlled Fusion and Plasma Physics, Kiev, Vol. 20, Part C, 763 (1996).

[18]R.C. Isler, R.W. Wood, C.C. Klepper, N.H. Brooks, M.E. Fenstermacher, A.W. Leonard, Phys. Plasmas **4**, 355 (1997).

[19]M.E. Fenstermacher, W.H. Meyer, R.D. Wood, D.G. Nilson, R. Ellis, and N.H. Brooks, Rev. Sci. Intrum. **68**, 974 (1997).

[20]M.E. Fenstermacher, S.L. Allen, N.H. Brooks, D.A. Buchenauer, T.N. Carlstrom, J.W. Cuthbertson, E.J. Doyle, T.E. Evans, P.M. Garbet, R.W. Harvey, D.N. Hill, A.W. Hyatt, R.C. Isler, G. Jackson, R.A. James, R. Jong, C.C. Klepper, C.J. Lasnier, A.W. Leonard, M.A. Mahdavi, R. Maingi, W.H. Meyer, R.A. Moyer, D.G. Nilson, T.W. Petrie, G.D. Porter, T. L. Rhodes, M.J. Schaffer, R.D. Stambaugh, D.M. Thomas, S. Tugarinov, M.R. Wade, J.G. Watkins, W.P. West, D.G. Whyte, R.D. Wood, Phys. Plasmas **4**, 1761 (1997).

[21]D.E. Post, J. Nucl. Mater. **220-222**, 143 (1995).

[22]R.D. Wood, S.L. Allen, M.E. Fenstermacher, D.N. Hill, Miller, R.C. Isler, A.W. Leonard, W.P. West, Bull. Am. Phys. Soc. **42**, 1844 (1997).

[23]R.C. Isler, G.R. Mckee, N.H. Brooks, W.P. West, M.E. Fenstermacher, R.W. Wood, Phys. Plasmas **4**, 2989 (1997).

[24]D. Lumma, J.L. Terry, B. Lipshultz, Phys. Plasmas **4**, 2555 (1997).

[25]J. L. Terry, B. Lipshultz, D. Lumma, B. LaBombard, D. Pappas, 24th European Physical Society Conf. on Controlled Fusion and Plasma Physics, Berchtesgaden, Vol. 21A, 573 (1997).

[26]B. Napiontek, U. Wenzel, K. Behringer, D. Coster, J. Gafert, R. Schneider, A. Thoma, M. Weinlich, 24th European Physical Society Conf. on Controlled Fusion and Plasma Physics, Berchtesgaden, Vol. 21A, 1413 (1997).

[27]J. L. Terry , Phys. Plasmas, This issue.

[28]S.I. Kracheninnikov, D.A. Knoll, Contrib. Plasma Phys. **36**, 266 (1996).

[29]T. Rognlien, J.L. Milovich, M.E. Rensink, and G.D. Porter, J. Nucl. Mater. **196-198**, 347 (1992).

[30]F. Wising, S.I. Krasheninnikov, D.J. Sigmar, D.A. Knoll, and T.D. Rognlien, Bull. Am. Phys. Soc. **40**, 1879 (1995).

[31]G.D. Porter, S.L. Allen, M. Brown, M.E. Fenstermacher, D.N. Hill, R.A. Jong, A.W. Leonard, D.G. Nilson, M.E. Rensink, T.D. Rognlien, G.R. Smith and the DIII–D Team, Phys. Plasmas **3**, 1967 (1996).

ACKNOWLEDGMENT

Work supported by U.S. Department of Energy under Contract Nos. DE-AC03-89ER51114, W-7405-ENG-48, DE-AC05-96OR22464, DE-AC04-94AL85000, and Grant No. DE-FG03-95ER54294.

Report Number (14) CA--A22787
CONF-971103--

Publ. Date (11) 199801
Sponsor Code (18) DOE/ER, XF
UC Category (19) UC-400, DOE/ER

DOE